REPORT DOCUMENTATION PAGE

AFRL-SR-AR-TR-02-

0209

1. REPORT DATE (DD-MM-YYYY)	2. REPORT TYPE	3. DATES COVERED (From - To)
06/18/2002	Final Report	11/1/97-4/30/01

4. TITLE AND SUBTITLE

High Speed All Optical Switching in Semiconductor-Oxide Microcavities via Coherent Control of Excitons

5a. CONTRACT NUMBER

5b. GRANT NUMBER
F49620-97-1-0533

5c. PROGRAM ELEMENT NUMBER

6. AUTHOR(S)

Theodore B. Norris

5d. PROJECT NUMBER

5e. TASK NUMBER

5f. WORK UNIT NUMBER

7. PERFORMING ORGANIZATION NAME(S) AND ADDRESS(ES)

Regents of the University of the Michigan
3003 South State St.
Ann Arbor, MI 48109-1287

8. PERFORMING ORGANIZATION REPORT NUMBER
036339F

9. SPONSORING / MONITORING AGENCY NAME(S) AND ADDRESS(ES)

Gernot S. Pomrenke,
Air Force Office of Scientific Research
Ballston Common Towers II, 801 N. Randolph St. Rm 732
Arlington, VA 22203-1977

10. SPONSOR/MONITOR'S ACRONYM(S)

11. SPONSOR/MONITOR'S REPORT NUMBER(S)

12. DISTRIBUTION / AVAILABILITY STATEMENT

UL

DISTRIBUTION STATEMENT A
Approved for Public Release
Distribution Unlimited

13. SUPPLEMENTARY NOTES

14. ABSTRACT

We have carried out an extensive series of experiments on coherent control of semiconductor quantum microcavities. In these experiments, a phase-locked femtosecond optical pulse pair is used to excite the lower normal mode (cavity polariton), thereby controlling the reflection of a signal pulse tuned to the upper normal mode. Such a controlled reflection may be used as an all-optical switch with picosecond switching time. We have demonstrated that the effect of the microcavity is to provide a huge enhancement of the coherently controlled response compared to bare quantum wells. We have investigated in detail the microscopic physical processes responsible for the nonlinear optical response; the measured response fits well with theories based on the electron-hole Hamiltonian in the coherent-$\chi(5)$ and 2^{nd}-Born approximations. The physical limits to the coherent control are determined by excitation-induced dephasing; this limits the applicability of the switch in practical terms. We have discovered that the use of phase-locked excitation pulses is that one can generate novel intraband coherences in the quantum wells, arising from true quantum correlations between the cavity field and the carrier populations. The discovery of this effect was perhaps the first genuinely quantum otical effect observed in semiconductor microcavities.

15. SUBJECT TERMS

16. SECURITY CLASSIFICATION OF:			17. LIMITATION OF ABSTRACT	18. NUMBER OF PAGES	19a. NAME OF RESPONSIBLE PERSON
a. REPORT	b. ABSTRACT	c. THIS PAGE		29	Theodore Norris
					19b. TELEPHONE NUMBER (include area code) 734-764-9269

Standard Form 298 (Rev. 8-98)
Prescribed by ANSI Std. Z39.18

High-Speed All-Optical Switching in Semiconductor Microcavities via Coherent Control of Excitons

grant # F49620-97-1-0533

Final Report

submitted to Dr. Gernot Pomrenke
Air Force Office of Scientific Research

Principal Investigator:

Prof. Theodore B. Norris
Center for Ultrafast Optical Science
EECS Department, University of Michigan
2200 Bonisteel Blvd, Ann Arbor, MI 48109-2099
(313) 764-9269 tnorris@eecs.umich.edu

2. Objectives

The overall objectives of the proposed three-year program were to investigate the coherent control of semiconductor normal-mode microcavities for potential applications in all-optical switching. We have carried out an exhaustive investigation of coherent control using phase-locked femtosecond optical pulses. We have detemined the limiting factor governing the coherent control for all-optical switching to be excitation-induced dephasing [EID] (published in Appl. Phys. Lett.). We have demonstrated picosecond switching using phase-controlled pulses, but the EID in present quantum-well-based device structures will limit the practicality of such a switch; potentially future quantum-dot based microcavities will eliminate this problem.

As part of the program, we carried out an extensive series of experiments investigating the detailed microscopic processes responsible for the nonlinear optical response of the microcavity system. This work was performed in collaboration with the theory group of Stephan Koch, and has been submitted to Phys. Rev. B (since it is not yet published, we have included a detailed discussion in section 4 of this report). We have found excellent agreement with microscopic models based on coherent-$\chi^{(5)}$ and 2nd-Born models to include the effects of incoherent carriers.

We also performed a series of experiment which probe the normal mode dynamics via the resonantly excited luminescence, or secondary emission. We developed a preliminary phenomenological based on scattering of cavity-polariton populations which showed a high degree of coherent control in the system, and the ability to control the emission between the normal modes. Since the concept of polariton populations is fundamentally problematic from a basic theoretical point of view, we have been working with Mackillo Kira and Stephan Koch to understand the results from a microscopic theory based on the fully quantized semiconductor luminescence equations. These results are still being written up for Phys. Rev. Lett.

The most surprising discovery of this program was that coherent control could lead to the generation of a completely novel kind of coherence in the system: namely intraband coherences driven by quantum correlations between the cavity field and the carrier populations. These intraband coherences turned out to be central to understanding the nature of light emission in semiconductors. This effect also could be thought of as the first truly quantum-optical effect (i.e. requiring the quantization of the electromagentic field) in semiconductor microcavity physics; as such it may potentially lead to new and interesting phenomena and applications (such as squeezing and entanglement) in microcavities. This work was published in Phys. Rev. Lett.

3. Status of Effort

The three-year research program has been completed. As discussed in the previous section, we still have two papers in the pre-publication stage; all other work carried out under the program have been published (see sections 6 and 7 of this document for a list).

4. Accomplishments/New Findings

The following discusses in detail the findings of the final year of the program which have not yet been published.

5. Personnel

Prof. Theodore B. Norris
Yun-Shik Lee (postdoctoral researcher)
Angelo Mazzocco (undergraduate)

6. Publications

M. Kira, F. Jahnke, S.W. Koch, Y.-S. Lee, T.B. Norris, G. Khitrova, and H.M. Gibbs, "Coherent Control of Secondary Emission from Normal Mode Microcavities," manuscript in preparation for Phys. Rev. Lett.

Y.-S. Lee, T.B. Norris, F. Jahnke, C. Sieh, T. Meier, S.W. Koch, G. Khitrova, and H.M. Gibbs, "Coherent Optical Nonlinearities in Normal-Mode Microcavities," submitted to Phys. Rev. B.

Y.S. Lee, T.B. Norris, A. Maslov, D.S. Citrin, J. Prineas, G. Khitrova, and H.M. Gibbs, "Large-Signal Coherent Control of Normal Modes in Quantum-Well Semiconductor Microcavity," Appl. Phys. Lett. 78, 3941 (2001).

Y.-S. Lee, T.B. Norris, A.V. Maslov, and D.S. Citrin, "Coherent Control and Nonlinear Interactions o fSemiconductor Cavity Polaritons," in Ultrafast Phenomena XII, Proceedings of the Twelfth International Conference, Charleston, 2000, ed. By T. Elsaesser, S. Mukamel, M.M. Murnane, and N.F. Scherer, Springer Series in Chemical Physics vol. 66, (Springer-Verlag, Berlin, 2000), p. 39.

Y.-S. Lee, T.B. Norris, M. Kira, F. Jahnke, S.W. Koch, G. Khitrova, and H.M. Gibbs, "Nondegenerate Coherent Control of Polariton Modes in a Quantum Well Semiconductor Microcavity," Phys. Stat. Solidi. (b) 221, 121-125 (2000).

Y.-S. Lee, T.B. Norris, M. Kira, F. Jahnke, S.W. Koch, G. Khitrova, and H.M. Gibbs, "Intraband Quantum Correlations in Semiconductor Quantum Well Microcavity," Phys. Stat. Solidi.(a) 178, 391 (2000).

Y.-S. Lee, T.B. Norris, M. Kira, F. Jahnke, S.W. Koch, G. Khitrova, and H.M. Gibbs, "Quantum Correlations and Intraband Coherences in Semiconductor Cavity QED," Phys. Rev. Lett. 83, 5338 (1999).

Y.-S. Lee, T.B. Norris, A. Maslov, D.S. Citrin, J. Prineas, G. Khitrova, and H.M. Gibbs, "Coherent Control of Normal Modes in a Quantum-Well Semiconductor Microcavity," Optics and Photonics News 9, (no.7) 60 (1998).

T.B. Norris, "Excitons in Strongly Coupled Microcavities," in Semiconductor Quantum Optoelectronics: From Quantum Physics to Smart Devices, ed. by A. Miller and D. Finlayson (Institute of Physics, 1999), pp.121-150.

7. Interactions/Transitions

(a) Conference Publications:

Y.S. Lee, T.B. Norris, G. Khitrova, H.M. Gibbs, C. Sieh, T. Meier,S.W. Koch, and F. Jahnke, "Coherent Optical Nonlinearities in Normal Mode Microcavities," paper QThL2 presented at QELS, Baltimore, 2001.

Y.-S. Lee, T.B. Norris, A.V. Maslov, and D.S. Citrin, "Coherent Control and Nonlinear Interactions o fSemiconductor Cavity Polaritons," presented at the Ultrafast Phenomena Conference, Charleston, 2000.

Y.-S. Lee, T.B. Norris, M. Kira, F. Jahnke, S.W. Koch, A. Maslov, D.S. Citrin, J. Prineas, G. Khitrova, and H.M. Gibbs, "Coherent Control and Quantum Correlations in Semiconductor Microcavities," invited paper presented at the SPIE Photonics West'00 International Symposium on Ultrafast Phenomena in Semiconductors IV, San Jose, January 2000.

Y.S. Lee, T.B. Norris, M. Kira, F. Jahnke, S.W. Koch, G. Khitrova, and H.M. Gibbs, "Qauntum Correlation Induced Intraband Coherences in a Quantum-Well Microcavity," paper QtuB6, , Quantum Electronics and Laser Science Conference, San Francisco, May 2000.

Y.S. Lee, T.B. Norris, M. Kira, F. Jahnke, S.W. Koch, G. Khitrova, and H.M. Gibbs, "Coherent Control of Cavity-Polariton Secondary Emission, paper QThQ4, Quantum Electronics and Laser Science Conference, San Francisco, May 2000.

T.B. Norris, "Coherent Control of Excitons in Semiconductor Microcavities," invited paper QTuD2, OSA Topical Meeting on Quantum Optoelectronics, Snowmass, April 1999.

T.B. Norris, "Coherent Control of Strongly Coupled Semiconductor Microcavities," invited paper presented at ILS-99, Santa Clara, September 1999.

Y.-S. Lee, T.B. Norris, M. Kira, F. Jahnke, S.W. Koch, A. Maslov, D.S. Citrin, J. Prineas, G. Khitrova, and H.M. Gibbs, "Correlations and Coherent Control of Normal Modes in a Microcavity," International Conference on Excitons in Confined Systems, Ascona, Switzerland, 1999.

Y.-S. Lee, T.B. Norris, A. Maslov, D.S. Citrin, J. Prineas, G. Khitrova, and H.M. Gibbs, "Coherent Control of Polaritons in a Quantum-Well Microcavity," paper QMF1, QELS, Baltimore, 1999.

Y.-S. Lee, A. Maslov, T.B. Norris, D.S. Citrin, J. Prineas, G. Khitrova, and H.M. Gibbs, "Coherent Control of Normal Modes in Quantum Well Semiconductor Microcavity," paper FH6, OSA/ILS-XIV, 14th Interdisciplinary Laser Science Conference, Baltimore, 1998.

T.B. Norris, "Coherent Control of Normal Modes in Strongly Coupled Microcavities," invited paper presented at the International Workshop on Coherent Control of Carrier Dynamics in Semiconductors," University of Illinois at Chicago, May 1998.

Y.-S. Lee, T.B. Norris, A. Maslov, D.S. Citrin, J. Prineas, G. Khitrova, and H.M. Gibbs, "Coherent Control of Normal Modes in a Semiconductor Microcavity," postdeadline paper QPD3, International Quantum Electronics Conference, San Francisco, 1998.

8. Inventions/Patent Disclosures

None

9. Honors/Awards

None

ACCOMPLISHMENTS AND NEW FINDINGS

Coherent control and optical nonlinearity of quantum-well microcavity

1 Overview

The objective of this project is to accomplish ultrafast all-optical switching in devices based on semiconductor quantum-well structures. In previous years, we have demonstrated that the switching rates are able to reach as high as 100 Gigabits/sec which is at least 10 times faster than most advanced current technology [1, 2, 3]. The physical principle of the optical switch is the coherent control of exciton population in semiconductor quantum-well(QW). We demonstrated that the signal of coherent control of the cavity-polariton modes of a QW microcavity is at least three orders of magnitude larger than of the exciton of multiple QW, thus the signal can be observed in the direct measurement of reflectivity without any complex signal amplification scheme [3]. The large signal and simple detection scheme make it possible for us to build compact device for optical switching. Besides, due to the mode-coupling of cavity and exciton in QW microcavity, the signal frequency can be separated from control frequency, which prevents signal cross-talk and coherent artifacts[4].

In order for profound understanding of the coherent control in QW microcavity, We have investigated various optical nonlinearities of the system to characterize the optical properties of the samples. As the results of the thorough investigation, we achieved fundamental understandings of the carrier dynamics and optical properties of the light-matter coupled system. We summarize the findings in the following sections.

2 Coherent control and nonlinear response of secondary emission

In the nonperturbative regime of quantum-well (QW) microcavities, the strong light-matter interaction results in the cavity polariton modes [5]. The normal modes of QW microcavity are often regarded as a coupled harmonic oscillator since the normal modes are equal admixture of exciton and cavity mode [6]. However, only the exciton mode is responsible for the optical nonlinearity of the QW microcavity, thus, whether the exciton mode is coherently controllable, or each normal mode can be controlled independently is a fundamental question. Besides, due to the cavity enhancement, high carrier density can be easily achieved in the QW microcavity. Thus, manybody interaction becomes crucial to understand the carrier dynamics of the cavity polaritons. Especially, the suppressed carrier scattering of the lower mode polaritons has been reported in several articles [7, 8, 9].

We have studied the coherent control of the polariton secondary emission from a QW microcavity, and investigated the nonlinear response of the emission. In order to see if only the exciton mode or each polariton mode is coherently controllable, we vary the temporal pump pulse separation, thus change the fringe frequency of the pump spectrum, and observe the secondary emission from

the sample. We refer to the emission as photoluminescence (PL) of normal modes. We also study the carrier-carrier interaction dynamics by investigating the intensity of the polariton secondary emission within the nonperturbative regime. We modulate the spectrum of the pump pulses using a pulse shaper, which enables us to pump each mode selectively, or both modes together. Our experimental results show the significant asymmetry in the PL of the lower and the upper polariton modes between the different pumping schemes (single and double modes pumping), which indicates an asymmetric carrier-carrier scattering mechanism of the normal modes.

The sample under investigation has two $In_{0.04}Ga_{0.96}As$ QW's embedded in the cavity of distributed Bragg reflectors (14 (16.5) periods of GaAs/AlAs on top (bottom) mirrors). The QW exciton resonance energy and linewidth are 1.487 ev and 0.7 meV at 10 K respectively. The normal mode splitting is 4.5 meV at zero detuning. The pump pulses were the output of a 82-MHz mode-locked Ti:sapphire laser producing 75-fs pulses centered at 831 nm. In the coherent control experiment, two pump pulses are generated by a Michelson interferometer, and the relative phase of the pump pulses is controlled by a piezoelectric translator. To investigate the asymmetry of normal modes PL intensity, a pulse shaper tailored the pump spectrum to enable that the pump pulse was resonant with only one normal mode. The spectral filter provided a very high contrast ratio, so that the intensity of the pump at the other mode was less than 10^{-3} of its intensity at the lower (upper) mode; hence any effects due to spectral overlap to the other mode is completely unobservable. The pump pulses irradiated on the sample near normal angle of incidence and the pump diameter was 35 μm. PL was collected at the normal angle and spectra were recorded on an optical multichannel analyzer.

In the linear response regime, the normal modes of QW microcavities are considered as ones of a coupled harmonic oscillator from the classical point of view. Though, it is not clear whether the classical perspective can be applied to the nonlinear optical regime, because only the excitonic components of the polariton modes are responsible for the nonlinear response of the normal modes. With the assumption of the classical picture applicable to the nonlinear case, the adjustment of the temporal separation of the two pump pulses makes it possible to control coherently each polariton mode with an independent manner, since each normal mode carries their own characteristic frequency. Figure 1 shows the time-integrated PL of the polariton modes when the temporal pump pulse separation (τ_{12}) is 0.0, 0.47, and 0.90 ps, and the detuning is 0.0 meV. The phase in the figures denotes the relative phase of the pump pulses at the resonance frequency of the lower mode polariton. In frequency domain, the fringe frequency of the two pump pulses is inversely proportional to τ_{12},thus the fringe frequency of τ_{12}=0.90 (0.47) ps corresponds to (twice of) the vacuum Rabi splitting of the QW microcavity. Figure 1 shows the coherently controlled PL of the normal modes for three different temporal separation of the two pump pulses. The cavity detuning is set to 0.5 meV where the PL intensities of the lower and the upper modes are comparable. In Fig. 1(a) when the two pump pulses are overlapped, thus, the fringe frequency is infinite, the pump pulse intensity varies with the cosine square of the relative phase of the two pump pulses. PL of the both modes goes up and down together as the phase varies. When τ_{12}=0.47 ps, then the fringe maximum of the two pump pulses falls into one of the normal modes resonance frequencies and the minimum hits the other. Figure 1(b) shows that the lower (upper) mode PL is maximum (minimum) when $\Delta\phi$=0. This indicates that each polariton mode is controlled coherently and independently. Finally, when we increase the pulse separation to 0.90 ps (Fig. 1(c)), the fringe maxima or minima fall into the resonance frequencies of the polariton modes simultaneously, and the PL intensity of the normal modes are maximum (minimum) at $\Delta\phi$=0 (π) together like when the two pump pulses are overlapped. The PL intensity of the polariton modes is almost identical with the one of τ_{12}=0.0 ps. Couple of features are noteworthy in Fig 1. First, there is a third peak when the two pulses are overlapped, and it disappears when the pulse separation is 0.9 ps even though the PL intensity of

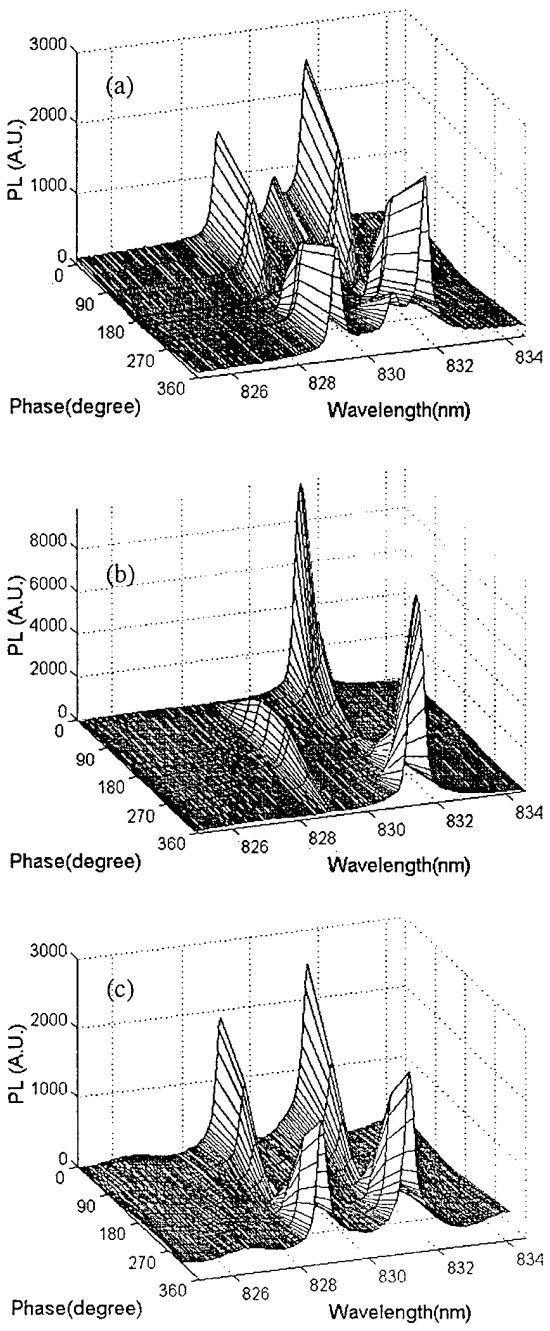

Figure 1: Coherently controlled PL spectra of the normal modes as a function of the relative phase between the two pump pulses when the temporal separation of the two pump pulses is (a) 0.0 (b) 0.47 and (c) 0.90 ps.

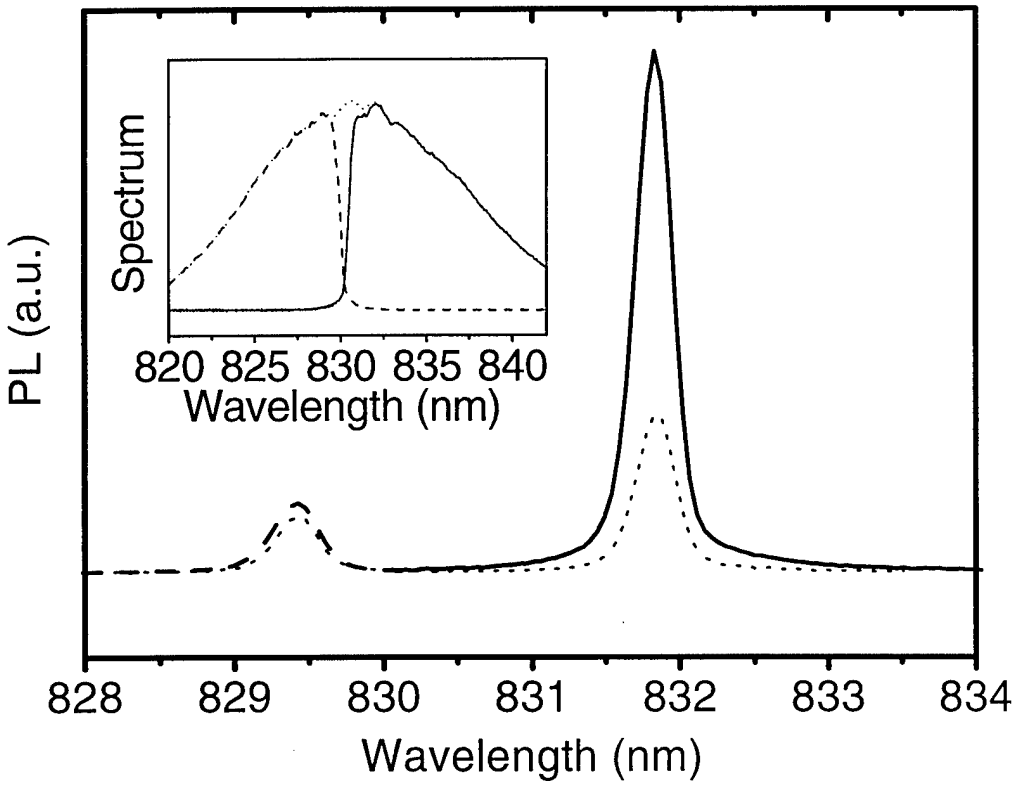

Figure 2: The secondary emission of the normal modes for the selective mode pumping. The pump fluence is 0.07 mJ/cm^2 when the both modes are pumped. Inset shows the pump spectra of single mode and both modes pumping.

the polariton modes is almost identical. According to Ell et al. [10], the third peak is sensitive to the density of the coherent polariton population. As the pulse separation increases, coherent population decreases because of the dephasing. Thus, the third peak decays with the pulse separation. Secondly, there is a striking phenomenon when the pulse separation is 0.47 ps. Figure 1(b) shows that the lower mode PL is much stronger than the upper mode PL when $\Delta\phi$=0. In this case, the upper mode PL intensity is almost same with the ones of τ_{12}=0.0 and 0.90 ps. Since the fringe maximum (minimum) of the pump pulses falls into the resonance frequency of the lower (upper) mode polariton when $\Delta\phi$=0, the experimental result implies that there is a significant increase of the lower mode PL intensity when only the lower mode is pumped.

To investigate the enhancement of the lower mode PL, we modify the pump spectrum of single pump pulse using the pulse shaper, which allows us to pump each mode selectively. or both modes together. The pump spectra are shown in the inset of Fig. 2 for each case. The modulation of the spectrum does not affect the pump intensity at the wavelength of the normal mode of the unmodulated side. Figure 2 shows the comparison between the lower and upper mode PL intensities when each mode or both modes are pumped when the cavity detuning is 0.0 meV and the pump fluence is 0.07 mJ/cm^2 where the differential reflectivity of the normal modes is less than 1 %. Clearly, the lower mode PL is substantially stronger when only the lower is pumped than of the both modes pumping, though the upper mode luminescence shows little effect of the different pumping schemes.

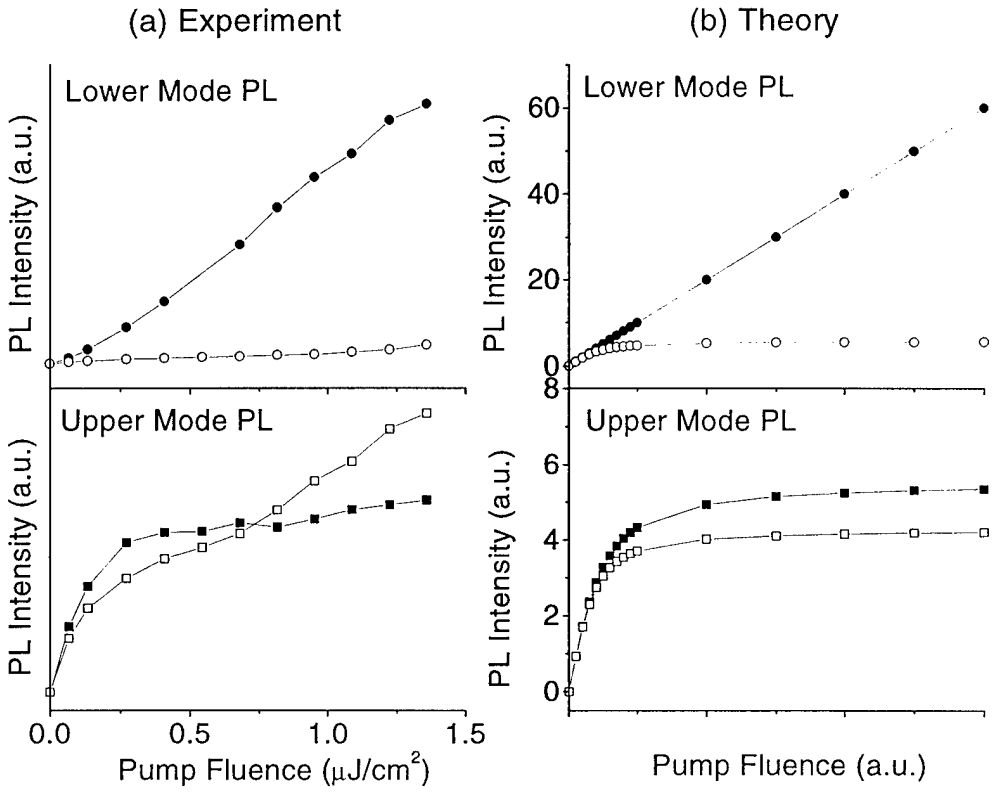

Figure 3: (a) experimental and (b) theoretical results of PL intensity vs. pump fluence. Lower mode PL when the lower mode (closed circle) and both modes (open circle) are pumped. Upper mode PL when the upper mode (closed square) and both modes (open square) are pumped.

For further study of the PL with different pumping schemes, we measured the time integrated PL of the normal modes for various pump intensity. Each pump pulse has the pulse duration of 85 fs(both modes pumping) and 190 fs (single mode pumping). Figure 3 shows the temporally and spectrally integrated PL intensity of polariton modes as a function of pump power when the detuning is 0.0 meV. In Fig 3(a), we compare the lower and upper mode PL intensities between the cases of the single mode and both modes pumping schemes. When the both modes are pumped simultaneously, the PL intensity shows some transition effect around 0.6 μJ/cm^2. According to the PL spectra analysis, the third peak appears around the same intensity and the PL intensity increases nonlinearly above the pump fluence. Our main discussion will be maintained below the critical fluence of the third peak. In the reflectivity measurement, the differential reflectivity of the normal modes spectra is less than 10 % below the critical pump fluence. In case of the single mode pumping, the pump fluence is measured before the pump spectrum is modified. The lower mode PL intensity of the lower mode only pumping scheme is much stronger than of pumping both modes. On the other hand, the upper mode PL intensity of the upper-mode only pumping scheme shows little difference with the one of both modes pumping scheme.

In order to understand the asymmetric behavior of the PL of the normal modes, we investigate the polariton dynamics as developing phenomenological rate equations of three-level system which consists of the lower mode, the upper mode and large in-plane momentum states which represent exciton reservoir.

$$\begin{aligned}
\frac{dN_u}{dt} &= P_u(t) - C_l\Gamma N_u - W_{uu}C_u^2N_u^2 - W_{ul}C_uC_lN_uN_l - W_{ux}C_uN_uN_x \\
\frac{dN_l}{dt} &= P_l(t) - C_u\Gamma N_l - W_{ll}C_l^2N_l^2 - W_{ul}C_uC_lN_uN_l - W_{lx}C_lN_lN_x \\
\frac{dN_x}{dt} &= -\Gamma_x N_x + 2W_{ul}C_uC_lN_uN_l + W_{lx}C_lN_lN_x + W_{ux}N_uN_x + W_{uu}C_u^2N_u^2 + W_{ll}C_l^2N_l^2
\end{aligned}$$

N_u and N_l represent the upper and lower mode polariton population respectively. N_x is the exciton population of the reservoir states. $P_u(t)$ and $P_l(t)$ describe the resonant pumping to the upper and lower mode. Since the pump beam is illuminated on the sample near normal angle of incidence and the pump spectrum is tuned to the normal modes resonantly, we assume that there are no carriers excited in the large in-plane momentum states. In a rough approximation, we describe the polariton decay rate by a linear combination of a cavity photon and an exciton decay rate weighted by the exciton and the photon component of mixed state [11]. C_u and C_l are the coefficients of exciton proportion of the upper and lower modes. Followings are the expressions for C_u and C_l:

$$\begin{aligned}
C_u &= \frac{1}{2}\frac{\sqrt{1+(\delta/g)^2}-(\delta/g)}{\sqrt{1+(\delta/g)^2}} \\
C_l &= \frac{1}{2}\frac{1}{\sqrt{1+(\delta/g)^2}(\sqrt{1+(\delta/g)^2}-(\delta/g))}
\end{aligned}$$

where δ is cavity detuning and g is $\hbar\Omega/2$ ($\hbar\Omega$ is normal mode splitting at zero detuning). Since cavity life time is much shorter than exciton life time, the upper mode and the lower mode decay rate can be approximated by $C_l\Gamma$ and $C_u\Gamma$ respectively where Γ is the cavity decay rate. W_{ij} is the scattering rate between the states i and j to transfer the states i and j to state x where i and j stands for u (upper mode), l (lower mode) and x (reservoir exciton states). Since only the exciton component of the polariton modes contributes to the carrier-carrier scattering, the

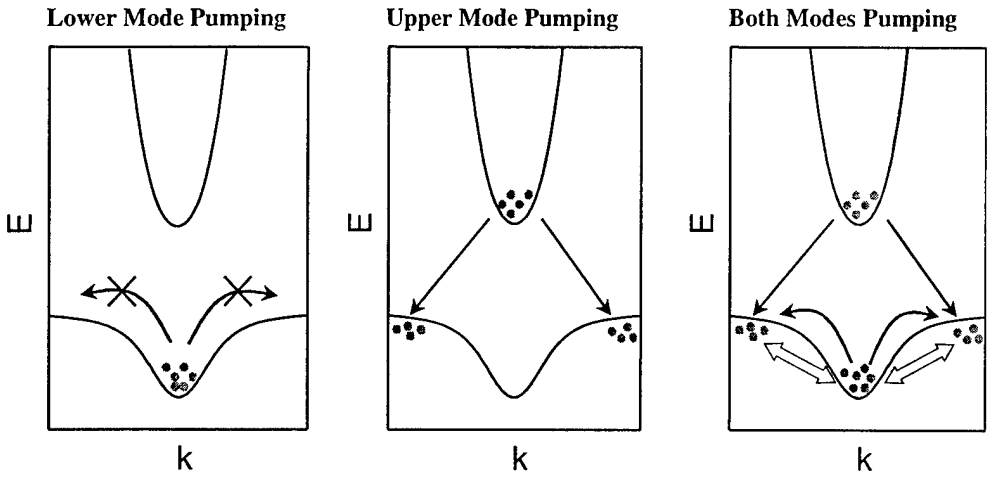

Figure 4: Schematics of the carrier-carrier scattering

scattering is weighted by the exciton component of the carriers. In the resonant pumping regime, we can neglect the scattering of reservoir excitons via acoustic phonons into the polariton states because the scattering rate ($\approx$0.002 ps ^{2}) [12] is substantially smaller than the radiative decay rate of the polariton modes.

We assumed that the transient PL intensity is proportional to the carrier density, thus the time-integrated PL intensity is calculated by temporally integrating the carrier density. Figure 3(b) shows the simulation result when the detuning is zero. The qualitative agreement between the experiment and the simulation is excellent. The simulation reproduces well the enhancement of the lower mode PL intensity when only the lower mode is pumped comparing with the one of the both modes pumping. Also, the upper mode PL intensity of only the upper mode pumping is not much different with the PL intensity when the both modes are pumped. Among the parameters, Γ, Γ_x, C_u, C_l are the well-known values. Thus, only the carrier scattering rates could be the fitting parameters. When only the lower mode is pumped, the PL intensity is linearly proportional to the pump fluence, thus all the nonlinear scattering terms are negligible. Especially, since the lower mode population is not zero, W_{LL} should be negligible. This can be easily understood because of the energy barrier from the lower mode polariton states to the exciton reservoir states. The suppression of the lower mode polariton scattering has been reported in [7, 8, 9]. W_{ul} also can be neglected because of the insensitivity of the upper mode PL to the pumping scheme. It turned out that W_{uu} and W_{lx} are dominant parameters. W_{ux} also affects the result of the simulation, but it is not as crucial as W_{uu} and W_{ul}. The nonlinear scattering terms cause the saturation of the PL intensity as the pump fluence increases. Followings are the parameters used in the simulation:

- C_l=C_u=0.5 : δ=0.0 meV
- Γ=0.2 ps^{-1} : T_c=5 ps
- Γ_x=0.005 : T_x=200 ps
- W_{uu}=W_{lx}=5 ps^{-1}, W_{ux}= 5 ps^{-1}, W_{ul}=0 ps^{-1}

Figure 4 shows the graphical schematics of the carrier scattering mechanism. Clearly, the scattering between the lower mode polariton and the reservoir exciton is the only mechanism to kick the lower mode polaritons out of the states. Thus, when only the lower-mode is pumped, large number

of lower-mode polaritons are remained in the initial state, so the PL intensity is quite strong. Also, due to the lack of the nonlinear scattering, the PL intensity increases linearly with the pump fluence. On the other hand, when the both modes are pumped simultaneously, the upper mode polaritons are scattered out of the states through the u-u and u-x scattering, and the lower-mode polaritons can be decayed to the reservoir states through l-x scattering. Thus, the PL intensity saturates at high excitation level. The negligible W_{ul} is crucial to explain the insensitivity of the upper mode PL to the pumping scheme because the insensitivity is the result of the lack of the direct scattering mechanism between the lower and upper mode. Primarily due to u-u scattering and also due to u-x scattering, the PL intensity saturates at high excitation level.

We demonstrate the coherent control of the cavity polariton PL, which confirms that each polariton mode can be controlled independently. The selective mode pumping scheme shows the stronger lower mode PL of the lower mode pumping than of the both modes pumping. On the other hand, the upper mode PL is insensitive to the pumping scheme. The asymmetric behavior of the polariton PL can be explained by the nonlinear carrier scattering. The rate equations of the three level system shows that the upper mode polariton scattering and the scattering between the reservoir exciton and the lower mode polariton is essential to explain the experimental results.

3 Coherent Optical Nonlinearities in Normal-Mode Microcavities

When a quantum-well (QW) exciton transition is resonant with a single mode of a high-Q microcavity, the linear response of the coupled system may be described in terms of normal modes or cavity polaritons [5]. The nonlinear response of these systems has often been discussed in terms of "polaritonic nonlinearities" [13, 14]. At the same time, tremendous progress has been made in understanding the microscopic origin of the polarization and intensity dependent nonlinear optical response in bare QWs, including self-consistent models of Coulomb correlation-induced nonlinearities in the coherent regime [6, 15, 16]. It is therefore desirable to investigate the nonlinearities in the normal-mode coupling (NMC) regime of QWs in a microcavity on the same level and to determine if the microscopic theories accounting for the bare-QW response also quantitatively account for the normal-mode nonlinear response.

In this section we discuss the coherent nonlinear optical response of a QW microcavity in the NMC regime. The changes in the reflection spectrum of a weak probe pulse are analyzed for various pumping conditions, where the selective excitation of only the lower or upper normal mode is compared with the case of both-mode excitation. The dependence on the pump intensity is studied for both co- and cross-circular polarization of probe and pump pulses. Furthermore, the temporal dependence of the nonlinearites on the pump-probe delay is discussed.

3.1 Theory in Second-Order Born Approximation

For a description of an external light field interacting with QWs embedded in a microcavity, the solution of Maxwells equations can be formulated in terms of the macroscopic QW polarization as discussed in detail in Ref. [6]. In a Bloch basis, the macroscopic QW polarization $\mathbf{P}_{QW}(z,t)$ can be calculated from the QW electron-hole transition amplitude $P_{\mathbf{k}}(t)$ according to

$$\mathbf{P}_{QW}(z,t) = |\xi(z)|^2 \frac{1}{S} \sum_{\mathbf{k}} \mathbf{d}_{cv}^* P_{\mathbf{k}}(t) + \text{c.c.} \tag{1}$$

where $\mathbf{k}$ is the in-plan carrier momentum, $\mathbf{d}_{cv}$ is the dipole matrix element, and S defines the normalization area of the QW. The space dependence of the macroscopic QW polarization is given

by the confinement wavefunction $|\xi(z)|^2$ where only resonant interaction with the lowest subband will be considered.

The equation of motion for the transition amplitude $P_{\mathbf{k}}(t)$

$$\left[i\hbar\frac{\partial}{\partial t} - \varepsilon^e_{\mathbf{k}}(t) - \varepsilon^h_{\mathbf{k}}(t)\right] P_{\mathbf{k}}(t) \;+\; \left[1 - f^e_{\mathbf{k}} - f^h_{\mathbf{k}}\right]\Omega_{\mathbf{k}}(t)$$
$$= -\,i\,\Gamma_{\mathbf{k}}\,P_{\mathbf{k}}(t) \;+\; i\sum_{\mathbf{k}'}\,\Gamma_{\mathbf{k},\mathbf{k}'}\,P_{\mathbf{k}+\mathbf{k}'}(t) \tag{2}$$

contains the renormalized single-particle energies of electrons ($a = e$) and holes ($a = h$),

$$\varepsilon^a_{\mathbf{k}}(t) = \epsilon^a_{\mathbf{k}} - \frac{1}{S}\sum_{\mathbf{k}'}\,V_{\mathbf{k}-\mathbf{k}'}\,f^a_{\mathbf{k}'}(t), \tag{3}$$

and the renormalized optical Rabi energy

$$\Omega_{\mathbf{k}}(t) = \mathbf{d}_{cv}\,\mathbf{E}_{QW}(t) + \frac{1}{S}\sum_{\mathbf{k}'}\,V_{\mathbf{k}-\mathbf{k}'}\,P_{\mathbf{k}'}(t). \tag{4}$$

where $V_{\mathbf{k}}$ is the quantum-well matrix element of the Coulomb potential and $\mathbf{E}_{QW}(t)$ is the optical field at the QW position, that has to be calculated self-consistently from Maxwells equations.

The occupation probabilities for electrons and holes $f^{e,h}_{\mathbf{k}}(t)$ can be obtained from the kinetic equation

$$i\hbar\frac{\partial}{\partial t}f^a_{\mathbf{k}}(t) \;+\; \Omega_{\mathbf{k}}(t)P^*_{\mathbf{k}}(t) - \Omega^*_{\mathbf{k}}(t)P_{\mathbf{k}}(t) \tag{5}$$
$$= \;i\left\{\Sigma^{in,a}_{\mathbf{k}}(t)\left[1 - f^a_{\mathbf{k}}(t)\right] - \Sigma^{out,a}_{\mathbf{k}}(t)f^a_{\mathbf{k}}(t) + \Sigma^{pol,a}_{\mathbf{k}}(t)\right\}.$$

Without the terms on the RHS, which will be discussed later in this section, Eqs. (2) and (5) are the semiconductor Bloch equations in Hartree-Fock approximation. Two-level Bloch equations for free-carrier transitions of the individual k-states are recovered, when all Coulomb terms are dropped. On the other hand, the Hartree-Fock Coulomb interaction introduces excitonic resonances, since in the absence of population effects, Eqs. (2) and (4) reduce to a momentum-space Schrödinger equation for the exciton relative motion.

To describe a pump-probe situation with two optical field components propagating in directions $\mathbf{k}_{pump}$ and $\mathbf{k}_{probe}$, a Fourier decomposition can be used [17]

$$\mathbf{E}^{total}(\mathbf{r},t) = \mathbf{E}(\mathbf{r},t)e^{i\mathbf{k}_{pump}\cdot\mathbf{r}} + \tilde{\mathbf{E}}(\mathbf{r},t)e^{i\mathbf{k}_{probe}\cdot\mathbf{r}}. \tag{6}$$

Since normal-mode effects are most prominent for optical fields perpendicular to the dielectric cavity mirrors, in the following we consider "nearly" normal incidence with a small angle between pump and probe beams.

In the weak-probe field limit, Eqs. (1)-(5) can be used to describe the nonlinear dynamics of the pump pulse where $\mathbf{P}_{QW}(z,t)$ and $P_{\mathbf{k}}(t)$ are now the pump-field induced macroscopic QW polarization and transition amplitude, and $\mathbf{E}_{QW}(t)$ is the spatial Fourier component of the pump field at the QW position.

Assuming that the probe field is weak such that only terms linear in the probe field have to be considered, probe field induced changes of the carrier occupation probabilities $f^{e,h}_{\mathbf{k}}$ can be neglected. However, the combined action of pump and probe fields (and their induced polarization components) leads to Fourier components of the carrier population $\delta f^{e,h}_{\mathbf{k}} \propto e^{i(\mathbf{k}_{probe}-\mathbf{k}_{pump})\cdot\mathbf{r}}$ which are related to

population pulsations [18]. These Fourier components enable the scattering of the pump field into probe direction as well as coupling the pump-induced polarization to the probe field. They are also responsible for a diffracted four-wave mixing signal which will not be considered in the following.

As for the pump pulse, the reflected and transmitted field of the probe pulse can be obtained from Maxwells equations using the Fourier component of the macroscopic QW polarization for the probe field

$$\tilde{\mathbf{P}}_{QW}(z,t) = |\xi(z)|^2 \frac{1}{S} \sum_{\mathbf{k}} \mathbf{d}_{cv}^* \tilde{P}_{\mathbf{k}}(t) + \text{c.c.} \tag{7}$$

The equation of motion for the corresponding transition amplitude,

$$\begin{aligned} \left[i\hbar \frac{\partial}{\partial t} - \varepsilon_{\mathbf{k}}^e(t) - \varepsilon_{\mathbf{k}}^h(t) \right] \tilde{P}_{\mathbf{k}}(t) \;\; + \;\; & \left[1 - f_{\mathbf{k}}^e - f_{\mathbf{k}}^h \right] \tilde{\Omega}_{\mathbf{k}}(t) \\ & - \left[\tilde{\varepsilon}_{\mathbf{k}}^e(t) + \tilde{\varepsilon}_{\mathbf{k}}^h(t) \right] P_{\mathbf{k}}(t) - \left[\delta f_{\mathbf{k}}^e + \delta f_{\mathbf{k}}^h \right] \Omega_{\mathbf{k}}(t) \\ = & - i\,\Gamma_{\mathbf{k}}\, \tilde{P}_{\mathbf{k}}(t) \;+\; i \sum_{\mathbf{k}'} \Gamma_{\mathbf{k},\mathbf{k}'}\, \tilde{P}_{\mathbf{k}+\mathbf{k}'}(t) \\ & - i\,\tilde{\Gamma}_{\mathbf{k}}\, P_{\mathbf{k}}(t) \;+\; i \sum_{\mathbf{k}'} \tilde{\Gamma}_{\mathbf{k},\mathbf{k}'}\, P_{\mathbf{k}+\mathbf{k}'}(t), \end{aligned} \tag{8}$$

contains the renormalized optical Rabi energy of the probe field

$$\tilde{\Omega}_{\mathbf{k}}(t) = \mathbf{d}_{cv}\, \tilde{\mathbf{E}}_{QW}(t) + \frac{1}{S} \sum_{\mathbf{k}'} V_{\mathbf{k}-\mathbf{k}'}\, \tilde{P}_{\mathbf{k}'}(t) \tag{9}$$

where $\tilde{\mathbf{E}}_{QW}(t)$ is the probe field at the QW position.

With the last term on the LHS of Eq. (8), that contains the $\delta f_{\mathbf{k}}^{e,h}$ Fourier components of the carrier populations, the generalized Rabi energy of the *pump* field directly influences the *probe* polarization. While the carrier occupation probabilities $f_{\mathbf{k}}^{e,h}$ lead to Hartree-Fock energy renormalizations according to Eq. (3), the additional Fourier components $\delta f_{\mathbf{k}}^{e,h}$ also introduce new renormalization terms

$$\tilde{\varepsilon}_{\mathbf{k}}^a(t) = -\frac{1}{S} \sum_{\mathbf{k}'} V_{\mathbf{k}-\mathbf{k}'}\, \delta f_{\mathbf{k}'}^a(t), \tag{10}$$

which mediate the direct entering of the *pump* induced transition amplitude $P_{\mathbf{k}}(t)$ on the LHS of Eq. (8). The quation of motion for the $\delta f_{\mathbf{k}}^{e,h}$ Fourier components of the carrier populations is given by

$$\begin{aligned} i\hbar \frac{\partial}{\partial t} \delta f_{\mathbf{k}}^a(t) \;\; + \;\; & \tilde{\Omega}_{\mathbf{k}}(t) P_{\mathbf{k}}^*(t) - \Omega_{\mathbf{k}}^*(t) \tilde{P}_{\mathbf{k}}(t) \\ = \;\; & i \Big\{ - \left[\Sigma_{\mathbf{k}}^{in,a}(t) + \Sigma_{\mathbf{k}}^{out,a}(t) \right] \delta f_{\mathbf{k}}^a(t) \\ + \;\; & \tilde{\Sigma}_{\mathbf{k}}^{in,a}(t) \left[1 - f_{\mathbf{k}}^a(t) \right] - \tilde{\Sigma}_{\mathbf{k}}^{out,a}(t) f_{\mathbf{k}}^a(t) + \tilde{\Sigma}_{\mathbf{k}}^{pol,a}(t) \Big\} \end{aligned} \tag{11}$$

where the second and third term on the LHS clearly reveal the combination of the *probe*-induced generalized Rabi energy with the *pump*-induced polarisation and vice versa as the driving source of $\delta f_{\mathbf{k}}^{e,h}$.

To consider the Coulomb interaction beyond the mean-field or Hartree-Fock level, we use in this section an approximation scheme where all correlation terms up to quadratic order in the screened Coulomb interaction are considered. This scheme allows the inclusion of interaction-induced dephasing due to carrier-carrier scattering and higher-order polarization interaction as well

as the corresponding dynamic energy renormalizations beyond the Hartree-Fock level. If a Markov approximation is used (which for the experimental situation discussed below practically does not influence the results), in the incoherent limit the correlation terms reduce to Boltzmann scattering integrals as well as generalized Coulomb enhancement and band-gap renormalization terms [6].

For coherent excitation conditions, the dynamics of the coherent excitonic polarization and the coherently driven carrier population under the influence of carrier-carrier scattering and nonlinear polarization interaction can be studied. Note that the derived terms are not limited to certain powers of the exciting field. On the other hand, the truncation in terms of powers of the screend Coulomb interaction excludes the consideration of biexcitonic bound states.

The aim of this paper is to demonstrate to what extend this so-called second-order Born approximation can be used to describe the coherent nonlinear response of QW excitons in a microcavity in comparison to the alternative approach discussed in Section 3.2.

The correlation terms on the RHS of Eq. (2) are either diagonal in the carrier momentum,

$$\begin{aligned}\Gamma_{\mathbf{k}} &= \frac{1}{S^2}\sum_{\mathbf{k}',\mathbf{k}''}\sum_{a,b=e,h} g\left(\varepsilon^a_{\mathbf{k}}+\varepsilon^b_{\mathbf{k}'+\mathbf{k}''}-\varepsilon^b_{\mathbf{k}''}-\varepsilon^a_{\mathbf{k}'+\mathbf{k}}\right)\left[W^2_{\mathbf{k}'}-\delta_{ab}W_{\mathbf{k}'}W_{\mathbf{k}-\mathbf{k}''}\right] \\ &\times \left[(1-f^b_{\mathbf{k}'+\mathbf{k}''})f^b_{\mathbf{k}''}f^a_{\mathbf{k}'+\mathbf{k}}+f^b_{\mathbf{k}'+\mathbf{k}''}(1-f^b_{\mathbf{k}''})(1-f^a_{\mathbf{k}'+\mathbf{k}})-P_{\mathbf{k}'+\mathbf{k}''}P^*_{\mathbf{k}''}\right], \qquad (12)\end{aligned}$$

or couple different $\mathbf{k}$-states,

$$\begin{aligned}\Gamma_{\mathbf{k},\mathbf{k}'} &= \frac{1}{S^2}\sum_{\mathbf{k}''}\sum_{a,b=e,h} g\left(-\varepsilon^a_{\mathbf{k}}-\varepsilon^b_{\mathbf{k}'+\mathbf{k}''}+\varepsilon^b_{\mathbf{k}''}+\varepsilon^a_{\mathbf{k}'+\mathbf{k}}\right)\left[W^2_{\mathbf{k}'}-\delta_{ab}W_{\mathbf{k}'}W_{\mathbf{k}-\mathbf{k}''}\right] \\ &\times \left[(1-f^a_{\mathbf{k}})(1-f^b_{\mathbf{k}'+\mathbf{k}''})f^b_{\mathbf{k}''}+f^a_{\mathbf{k}}f^b_{\mathbf{k}'+\mathbf{k}''}(1-f^b_{\mathbf{k}''})-P^*_{\mathbf{k}'+\mathbf{k}''}P_{\mathbf{k}''}\right], \qquad (13)\end{aligned}$$

where $W_{\mathbf{k}}$ is the screened Coulomb interaction which will be used in quasi-static RPA approximation (Lindhard formula), $g(\varepsilon)=\pi\delta(\varepsilon)+\mathcal{P}\frac{i}{\varepsilon}$, and $\mathcal{P}$ denotes that the principal value of the corresponding integral has to be taken.

To analyze the spin-polarization dependence of the scattering terms, additional spin indices of the carrier operator pairs contributing to $f^a_{\mathbf{k}}$ and $P_{\mathbf{k}}$ would have to be added. To keep the notation as simple as possibe, we discuss in the following only the results of such a consideration.

In Eqs. (12) and (13) we have assumed that the pump field is cirlularly polarized such that only one spin subsystem of the spin-degenerate electron and heavy-hole bands is excited. Then $f^a_{\mathbf{k}}$ and $P_{\mathbf{k}}$ are the occupation probabilities and transition amplitude for this spin-subsystem.

If the pump field equally excites both spin-subsystems, a factor of 2 has to be added to $W^2_{\mathbf{k}'}$ since the direct Coulomb interaction, described by this term, allows the scattering of carriers from one subsystem also with carriers from the other subsystem, which effectively doubles the scattering probability. However, the exchange interaction, described by $\delta_{ab}W_{\mathbf{k}'}W_{\mathbf{k}-\mathbf{k}''}$ is limited to carriers of the same spin-subsystem.

The corresponding correlation terms in Eq. (5) describe the changes of the carrier occupation probabilities $f^a_{\mathbf{k}}$ due to scattering of carriers into the state with momentum $\mathbf{k}$,

$$\begin{aligned}\Sigma^{in,a}_{\mathbf{k}} &= \frac{2\pi}{S^2}\sum_{\mathbf{k}',\mathbf{k}''}\sum_{b=e,h}\left[W^2_{\mathbf{k}'}-\delta_{ab}W_{\mathbf{k}'}W_{\mathbf{k}-\mathbf{k}''}\right] \\ &\times \delta\left(\varepsilon^a_{\mathbf{k}}+\varepsilon^b_{\mathbf{k}'+\mathbf{k}''}-\varepsilon^b_{\mathbf{k}''}-\varepsilon^a_{\mathbf{k}'+\mathbf{k}}\right)(1-f^b_{\mathbf{k}'+\mathbf{k}''})f^b_{\mathbf{k}''}f^a_{\mathbf{k}'+\mathbf{k}}, \qquad (14)\end{aligned}$$

due to scattering of carriers out of the k-state,

$$\begin{aligned}\Sigma^{out,a}_{\mathbf{k}} &= \frac{2\pi}{S^2}\sum_{\mathbf{k}',\mathbf{k}''}\sum_{b=e,h}\left[W^2_{\mathbf{k}'}-\delta_{ab}W_{\mathbf{k}'}W_{\mathbf{k}-\mathbf{k}''}\right] \\ &\times \delta\left(\varepsilon^a_{\mathbf{k}}+\varepsilon^b_{\mathbf{k}'+\mathbf{k}''}-\varepsilon^b_{\mathbf{k}''}-\varepsilon^a_{\mathbf{k}'+\mathbf{k}}\right)f^b_{\mathbf{k}'+\mathbf{k}''}(1-f^b_{\mathbf{k}''})(1-f^a_{\mathbf{k}'+\mathbf{k}}), \qquad (15)\end{aligned}$$

as well as due to nonlinear polarization interaction,

$$\begin{aligned}\Sigma_{\mathbf{k}}^{pol,a} &= \frac{1}{S^2}\sum_{\mathbf{k}',\mathbf{k}''}\sum_{b=e,h}\left[W_{\mathbf{k}'}^2-\delta_{ab}\,W_{\mathbf{k}'}W_{\mathbf{k}-\mathbf{k}''}\right]\\ &\times \left\{g\left(\varepsilon_{\mathbf{k}}^a+\varepsilon_{\mathbf{k}'+\mathbf{k}''}^b-\varepsilon_{\mathbf{k}''}^b-\varepsilon_{\mathbf{k}'+\mathbf{k}}^a\right)\left[\left(f_{\mathbf{k}}^a-f_{\mathbf{k}'+\mathbf{k}}^a\right)P_{\mathbf{k}'+\mathbf{k}''}P_{\mathbf{k}''}^*+c.c.,\right]\right.\\ &+ \left. g\left(\varepsilon_{\mathbf{k}}^{\bar{a}}+\varepsilon_{\mathbf{k}'+\mathbf{k}''}^b-\varepsilon_{\mathbf{k}''}^b-\varepsilon_{\mathbf{k}'+\mathbf{k}}^{\bar{a}}\right)\left[\left(f_{\mathbf{k}''}^b-f_{\mathbf{k}'+\mathbf{k}''}^b\right)P_{\mathbf{k}}P_{\mathbf{k}'+\mathbf{k}}^*+c.c.\right]\right\}. \qquad (16)\end{aligned}$$

For details, see Refs. [6, 19].

When the probe field has the same circular optical polarization as the pump field, the first set of correlation contributions to the *probe* polarization, $\Gamma_{\mathbf{k}}$ and $\Gamma_{\mathbf{k},\mathbf{k}'}$, are given by Eqs. (12) and (13), respectively. Note that with the last term of these equations, the pump-polarization $P_{\mathbf{k}}$ couples via direct and exchange Coulomb interaction to the probe polarization.

The $\delta f_{\mathbf{k}}^{e,h}$ Fourier components of the carrier populations lead to additional correlations terms, $\tilde{\Gamma}_{\mathbf{k}}$ and $\tilde{\Gamma}_{\mathbf{k},\mathbf{k}'}$, which also promote direct coupling of the pump-polarization to the probe signal in Eq. (8). For co-circular pump and probe polarization, one finds

$$\begin{aligned}\tilde{\Gamma}_{\mathbf{k}} &= \frac{1}{S^2}\sum_{\mathbf{k}',\mathbf{k}''}\sum_{a,b=e,h} g\left(\varepsilon_{\mathbf{k}}^a+\varepsilon_{\mathbf{k}'+\mathbf{k}''}^b-\varepsilon_{\mathbf{k}''}^b-\varepsilon_{\mathbf{k}'+\mathbf{k}}^a\right)\left[W_{\mathbf{k}'}^2-\delta_{ab}\,W_{\mathbf{k}'}W_{\mathbf{k}-\mathbf{k}''}\right]\\ &\times \left[-\delta f_{\mathbf{k}'+\mathbf{k}''}^b f_{\mathbf{k}''}^b f_{\mathbf{k}'+\mathbf{k}}^a+\delta f_{\mathbf{k}'+\mathbf{k}''}^b(1-f_{\mathbf{k}''}^b)(1-f_{\mathbf{k}'+\mathbf{k}}^a)\right.\\ &\quad +(1-f_{\mathbf{k}'+\mathbf{k}''}^b)\delta f_{\mathbf{k}''}^b f_{\mathbf{k}'+\mathbf{k}}^a-f_{\mathbf{k}'+\mathbf{k}''}^b\delta f_{\mathbf{k}''}^b(1-f_{\mathbf{k}'+\mathbf{k}}^a)\\ &\quad +(1-f_{\mathbf{k}'+\mathbf{k}''}^b)f_{\mathbf{k}''}^b\delta f_{\mathbf{k}'+\mathbf{k}}^a-f_{\mathbf{k}'+\mathbf{k}''}^b(1-f_{\mathbf{k}''}^b)\delta f_{\mathbf{k}'+\mathbf{k}}^a\\ &\quad \left.-\tilde{P}_{\mathbf{k}'+\mathbf{k}''}P_{\mathbf{k}''}^*\right], \qquad (17)\end{aligned}$$

$$\begin{aligned}\tilde{\Gamma}_{\mathbf{k},\mathbf{k}'} &= \frac{1}{S^2}\sum_{\mathbf{k}''}\sum_{a,b=e,h} g\left(-\varepsilon_{\mathbf{k}}^a-\varepsilon_{\mathbf{k}'+\mathbf{k}''}^b+\varepsilon_{\mathbf{k}''}^b+\varepsilon_{\mathbf{k}'+\mathbf{k}}^a\right)\left[W_{\mathbf{k}'}^2-\delta_{ab}\,W_{\mathbf{k}'}W_{\mathbf{k}-\mathbf{k}''}\right]\\ &\times \left[-\delta f_{\mathbf{k}}^a(1-f_{\mathbf{k}'+\mathbf{k}''}^b)f_{\mathbf{k}''}^b+\delta f_{\mathbf{k}}^a f_{\mathbf{k}'+\mathbf{k}''}^b(1-f_{\mathbf{k}''}^b)\right.\\ &\quad -(1-f_{\mathbf{k}}^a)\delta f_{\mathbf{k}'+\mathbf{k}''}^b f_{\mathbf{k}''}^b+f_{\mathbf{k}}^a\delta f_{\mathbf{k}'+\mathbf{k}''}^b(1-f_{\mathbf{k}''}^b)\\ &\quad +(1-f_{\mathbf{k}}^a)(1-f_{\mathbf{k}'+\mathbf{k}''}^b)\delta f_{\mathbf{k}''}^b-f_{\mathbf{k}}^a f_{\mathbf{k}'+\mathbf{k}''}^b\delta f_{\mathbf{k}''}^b\\ &\quad \left.-P_{\mathbf{k}'+\mathbf{k}''}^*\tilde{P}_{\mathbf{k}''}\right]. \qquad (18)\end{aligned}$$

Note that in comparison to Eq. (12) and (13) the Fourier component $\propto e^{i(\mathbf{k}_{probe}-\mathbf{k}_{pump})\cdot\mathbf{r}}$ are considered by means of $\delta f_{\mathbf{k}}^a$ as well as the combination of pump and probe-polarizations. Similarly, the additional correlation terms in Eq. (11) are given by

$$\begin{aligned}\tilde{\Sigma}_{\mathbf{k}}^{in,a} &= \frac{2\pi}{S^2}\sum_{\mathbf{k}',\mathbf{k}''}\sum_{b=e,h}\delta\left(\varepsilon_{\mathbf{k}}^a+\varepsilon_{\mathbf{k}'+\mathbf{k}''}^b-\varepsilon_{\mathbf{k}''}^b-\varepsilon_{\mathbf{k}'+\mathbf{k}}^a\right)\left[W_{\mathbf{k}'}^2-\delta_{ab}\,W_{\mathbf{k}'}W_{\mathbf{k}-\mathbf{k}''}\right]\\ &\times \left[-\delta f_{\mathbf{k}'+\mathbf{k}''}^b f_{\mathbf{k}''}^b f_{\mathbf{k}'+\mathbf{k}}^a+(1-f_{\mathbf{k}'+\mathbf{k}''}^b)\delta f_{\mathbf{k}''}^b f_{\mathbf{k}'+\mathbf{k}}^a+(1-f_{\mathbf{k}'+\mathbf{k}''}^b)f_{\mathbf{k}''}^b\delta f_{\mathbf{k}'+\mathbf{k}}^a\right], \qquad (19)\end{aligned}$$

$$\begin{aligned}\tilde{\Sigma}_{\mathbf{k}}^{out,a} &= \frac{2\pi}{S^2}\sum_{\mathbf{k}',\mathbf{k}''}\sum_{b=e,h}\delta\left(\varepsilon_{\mathbf{k}}^a+\varepsilon_{\mathbf{k}'+\mathbf{k}''}^b-\varepsilon_{\mathbf{k}''}^b-\varepsilon_{\mathbf{k}'+\mathbf{k}}^a\right)\left[W_{\mathbf{k}'}^2-\delta_{ab}\,W_{\mathbf{k}'}W_{\mathbf{k}-\mathbf{k}''}\right]\\ &\times \left[\delta f_{\mathbf{k}'+\mathbf{k}''}^b(1-f_{\mathbf{k}''}^b)(1-f_{\mathbf{k}'+\mathbf{k}}^a)-f_{\mathbf{k}'+\mathbf{k}''}^b\delta f_{\mathbf{k}''}^b(1-f_{\mathbf{k}'+\mathbf{k}}^a)-f_{\mathbf{k}'+\mathbf{k}''}^b(1-f_{\mathbf{k}''}^b)\delta f_{\mathbf{k}'+\mathbf{k}}^a\right]. \qquad (20)\end{aligned}$$

$$
\begin{aligned}
\tilde{\Sigma}^{pol,a}_{\mathbf{k}} &= \frac{1}{S^2}\sum_{\mathbf{k}',\mathbf{k}''}\sum_{b=e,h}\left[W^2_{\mathbf{k}'} - \delta_{ab}\,W_{\mathbf{k}'}W_{\mathbf{k}-\mathbf{k}''}\right] \\
&\times \Big\{ g\left(\varepsilon^a_{\mathbf{k}} + \varepsilon^b_{\mathbf{k}'+\mathbf{k}''} - \varepsilon^b_{\mathbf{k}''} - \varepsilon^a_{\mathbf{k}'+\mathbf{k}}\right) \\
&\quad \times \left[\left(f^a_{\mathbf{k}} - f^a_{\mathbf{k}'+\mathbf{k}}\right)\tilde{P}_{\mathbf{k}'+\mathbf{k}''}P^*_{\mathbf{k}''} + \left(\delta f^a_{\mathbf{k}} - \delta f^a_{\mathbf{k}'+\mathbf{k}}\right)P_{\mathbf{k}'+\mathbf{k}''}P^*_{\mathbf{k}''} + c.c.,\right] \\
&+ \; g\left(\varepsilon^{\bar{a}}_{\mathbf{k}} + \varepsilon^b_{\mathbf{k}'+\mathbf{k}''} - \varepsilon^b_{\mathbf{k}''} - \varepsilon^{\bar{a}}_{\mathbf{k}'+\mathbf{k}}\right) \\
&\quad \times \left[\left(f^b_{\mathbf{k}''} - f^b_{\mathbf{k}'+\mathbf{k}''}\right)\tilde{P}_{\mathbf{k}}P^*_{\mathbf{k}'+\mathbf{k}} + \left(\delta f^b_{\mathbf{k}''} - \delta f^b_{\mathbf{k}'+\mathbf{k}''}\right)P_{\mathbf{k}}P^*_{\mathbf{k}'+\mathbf{k}} + c.c.\right]\Big\}. \qquad (21)
\end{aligned}
$$

For opposite circular optical polarisation of pump and probe pulses various changes in the discussed equations are necessary:

(I) The $\delta f^{e,h}_{\mathbf{k}}$ Fourier components of the carrier populations do not occur since the electronic polarization driven in one spin-subsystem cannot couple to the optical field which excites the other spin-subsystem. Correspondingly, the diffraction of the pump field into probe direction and the nonlinear interaction of the pump-induced electronic polarization with the probe polarization are absent.

(II) From the spin-dependence of the involved carrier operators it follows that (only) in Eq. (8), and in the Hartee-Fock and correlation terms of this equation, $f^a_{\mathbf{k}}$ and $f^a_{\mathbf{k}'+\mathbf{k}}$ are belonging to the spin-subsystem the probe pulse is interaction with. Since for cross-circular pump-probe excitation the pump field does not populate this spin subsystem and the weak probe field does not lead to population effects, $f^a_{\mathbf{k}}$ and $f^a_{\mathbf{k}'+\mathbf{k}}$ are zero in Eq. (8) and in the Hartee-Fock and correlation terms of this equation. Hence there are no phase-space filling and energy renormalization contributions of the pump field to the probe signal and the interaction-induced dephasing will be reduced.

(III) The exchange contributions to the correlation terms $\propto \delta_{ab}\,W_{\mathbf{k}'}W_{\mathbf{k}-\mathbf{k}''}$ do not contribute in Eq. (8) since the exchange interaction does not couple different spin subsystems.

Note that all Hartree-Fock and correlation terms entering in Eqs. (2) and (5) are independent of the optical polarization of the probe field.

3.2 Theory in $\chi^{(3)}$ and $\chi^{(5)}$-Approximation

Following is the Hamilton operator of the system, $H = H_0 + H_C + H_I$, where H_0 is the one-particle operator (containing the bandstructure), H_C contains the many-body Coulomb interaction (in so-called monopole-monopole approximation), and H_I is the explicitly time-dependent interaction with a classical electromagnetic field E (in dipole approximation, reasonable enough e.g. for a quantum well). Without H_I, the semiconductor is in its ground state, i.e. there are no (conduction) electrons and no holes. That's what later allows us to treat E as a perturbation. The aim is to derive an equation of motion for the one-particle density matrix $\langle a^\dagger a\rangle$ via the Heisenberg equation $-i\frac{\partial}{\partial t}\cdot = [H,\cdot]$. We distinguish between conduction and valence electrons (or electrons and holes), as in the Hamiltonian H_I the electric field couples to interband transitions only. Thus, we start with an equation for the interband coherence ("polarization") $p(\equiv Y) = \langle a^\dagger_v a_c\rangle$. We find that p couples to the other one-particle density matrices $f_c(\equiv C) = \langle a^\dagger_c a_c\rangle$ and $f_v(\equiv D) = \langle a^\dagger_v a_v\rangle$, and also to two-particle density matrices of the type S and T (in the Axt/Victor notation). However, the "dynamics controlled truncation scheme" tells us how to expand these matrices into the purely coherent contributions p ("one transition"), and B ("two transitions"), and also, which terms to consider, if we want to include terms of a certain order in the electric field. Thus, we don't need equations for C and D. In third order ($\chi^{(3)}$), we also don't need any higher transitions (see Victor et al.), so all that's left to do is to calculate the equation for B and neglect all terms higher than third order therein. We end up (schematically - no sums and indices included) with the terms not

marked with an arrow on the transparency. We have a closed system for p and B, which are coupled via the electric field E and the Coulomb interaction V. The matrix T in the homogeneous part is just the single particle contribution from H_0, which in our case (one-dimensional real-space tight-binding model) consists of the site energies (on the diagonal), and the next-neighbor coupling of the sites (right next to the diagonal). The model also includes two different conduction and valence band spins each, together with the appropriate selection rules, in order to describe the different polarization configurations.

While B is just driven by Ep, the p-equation has both phase-space filling (Pauli) $E(1-p^*p)$ and Coulomb inhomogeneities Vp^*B. (In earlier publications, we made a point of separating B into the Hartree-Fock part pp and a remaining ("correlation") part $\overline{B}$. Leaving out $\overline{B}$, which is driven by Vpp, then directly yields the Semiconductor Bloch Equations.

When we go on to the next higher order ($\chi^{(5)}$), two things happen. First, we have to include more terms in the equations for p and B (surprisingly the ones marked by an arrow); second, the coherent three-transition type quantity, W , appears, for which one should also write an equation. W , however, is neglected in all numerical simulations, for the single reason that one can't handle it in reasonable time, because it is a six-point function. What's more, even the unbound two-excitons contained in B can not be properly resolved due to the smallness of our model system; this problem would become even more prominent for unbound three-excitons. On the other hand, bound solutions (triexcitons), are not expected to play an important role.

When calculating the pump-probe signal, we have two fields (pulses) E traveling in different directions. We then calculate p (and B) for each direction and order separately, which means we have a first order p in pump direction, a first order p in probe direction, higher order p's in probe direction, and also all the directions needed to construct these higher order signals. In all cases, terms quadratic or higher in the probe pulse are neglected (since it is supposed to be only a weak test pulse), that means a fifth order p consists of 4 times pump and 1 time probe. The detected signal in a given (in that case probe) direction is then built additively from the different orders in that direction ($p = p^{(1)} + p^{(3)} + p^{(5)}$).

$$\begin{aligned} -i\hbar\dot{p} &= -Tp + Vp + E - Ep^*p \\ &\quad +Ep^*p^*B + EB^*pp - Ep^*p^*pp - \frac{1}{2}EB^*B \\ &\quad +Vp^*B + Vp^*p^*pB - VB^*pB \end{aligned} \tag{22}$$

$$-i\hbar\dot{B} = -TB + VB + Ep - Ep^*B \tag{23}$$

3.3 Nonlinear Pump-Probe Experiments

The sample in these experiments has two $In_{0.04}Ga_{0.96}As$ QW's placed at the antinodes of a $3\lambda/2$ cavity formed by two 99.6%-reflectivity distributed Bragg reflectors (14 (16.5) periods of GaAs/AlAs on top (bottom) mirrors). The QW exciton transition at 1.487 eV (linewidth 0.7 meV) is resonant with the cavity mode at 10 K, where all experiments were performed. The normal-mode splitting on resonance is 4.5 meV. The output of 85-MHz mode-locked Ti:sapphire laser producing 75-fs pulses centered at 831 nm has been used as the light source of the pump-probe set up. The pump pulses were generated by spectral filtering the laser output. The pump pulse was selectively resonant with only the upper or lower mode, with pulse durations of 190-fs, or excites both modes simultaneously. The spectral filter provided a very high contrast ratio, so that the intensity of the pump (probe) at

the upper (lower) mode was less than 10^{-3} of its intensity at the lower (upper) mode; hence any effects due to spectral overlap of the pump and probe are completely unobservable. The pump and probe beams were overlapped on the sample at near normal incidence; the pump (probe) diameter was 35(20) μm, and the probe fluence was always less than 10^{-2} that of the pump. Probe reflectance spectra were recorded on an optical multichannel analyzer.

3.4 Probe Nonlinear Response in Coherent Regime

We investigated the optical nonlinear response of the normal modes in coherent regime. Figure 5 shows the probe reflectance spectra for co-circular configuration when the lower mode is excited. The probe time delay was set around 0 ps. The data were measured for various cavity detuning ($\delta \equiv E_c - E_{ex}$) and pump fluence conditions. Some features of the nonlinear responses are noteworthy. First, the lower-mode undergoes substantial lineshift to the blue side. The blueshift and the mode amplitude increase with pump fluence. The lineshift is more prominent in positive detuning than in negative detuning. Second, the upper-mode also shows the blueshift with much less amount. Unlike the lower-mode, the upper mode saturates and the linewidth broadens at high pump fluence. Overall, the normal mode splitting reduces at high carrier density, which may be accounted by the phase space filling. Third, a gain peak appears at the red side of the lower mode. The peak amplitude increases with the pump fluences. Its relative size to the lower mode is bigger and the linewidth is wider in the positive detuning than in the negative detuning.

The normal-mode spectra for cross-circular polarization are demonstrated in Fig. 6. The optical nonlinear responses show distinctive characteristics relying on the pump-probe polarization. The probe spectra for cross-circular configuration are less susceptible to the pump fluence than for co-circular polarization. Furthermore, the nonlinear response is weaker in negative detuning than in positive detuning. The gain peak for the co-circular polarization is absent for cross-circular excitation and a slight red shift occurs. The prominent feature of the cross-circular configuration is the appearance of the new resonance at the red side of the upper mode. The new mode may be accounted by bi-excitonic transition. The bi-excitonic mode is not noticeable up to a certain pump fluence. The critical pump fluence increases as the cavity detuning, because the bi-excitonic binding energy increases with the cavity detuning. It is clearly shown in the data that the bi-excitonic binding energy in positive detuning is bigger than in negative detuning. With increasing carrier density, the biexcitonic mode grows as the upper mode fades away, because of the depletion of the ground states and the increase of the lower-mode population. When the positive detuning is over a certain limit (>0.9 meV), the biexcitonic mode does not appear even at high excitation level. Instead, a new spectrum emerges at the red side of the lower mode.

The semiconductor Bloch equations incorporated with phenomenological excitation induced dephasing (EID) has been applied to account for many optical nonlinear responses in QW system. The model can account for the reduction of the mode splitting and the spectral broadening in QW microcavity system, but it fails to explain the other features we have observed in the experiment. Thus, the Coulomb interaction terms beyond the Hartree-Fock level are required to account for the foremost normal-mode nonlinearities such as the lineshift and the gain peak for co-circular excitation and the bi-excitonic mode for cross-circular exctation.

The calculations with Coulomb correlations in second-order Born approximation are shown in Fig. 7. The Rabi energy of the pump pulse - in units of the Rydberg energy - refers to the pulse before the blue side of the spectrum (about 45 %) is blocked. The calculated results reproduce the gain at the red side of the lower mode for co-circular polarization. Like in the experiment, this gain is absent for cross-circular polarization. Co-circular polarization and strong pumping leads to oscillations in the probe reflection spectra due to diffraction of the pump pulse in probe direction

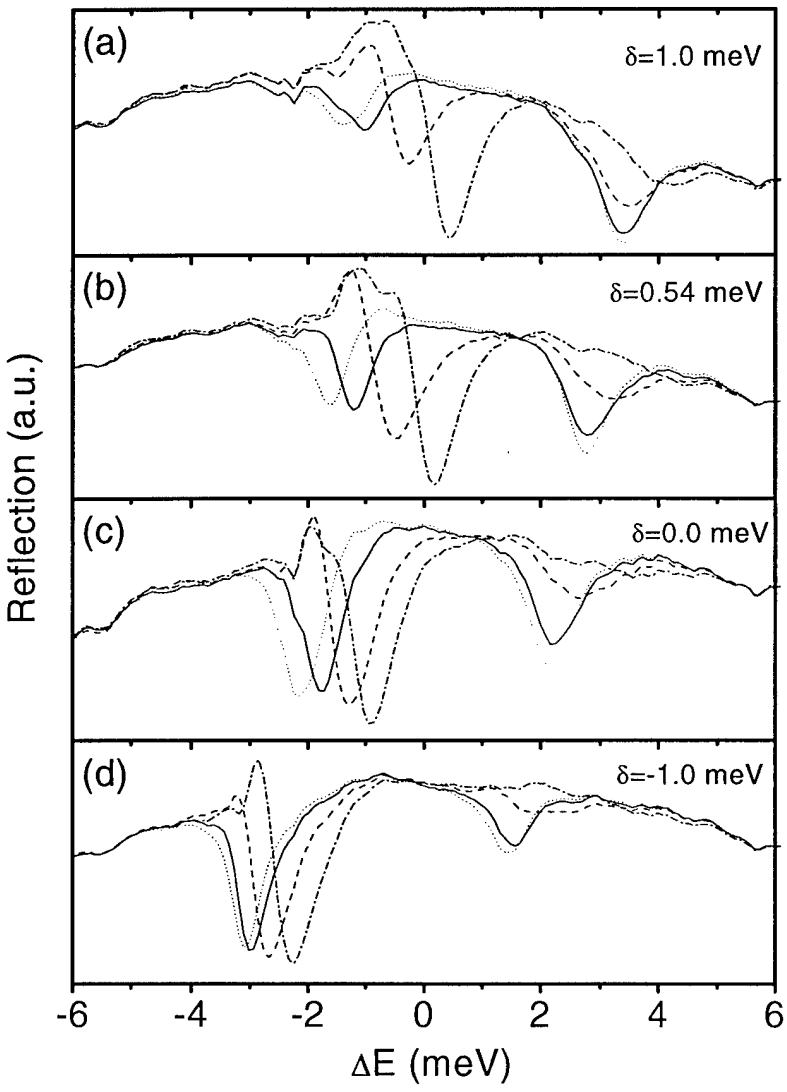

Figure 5: Measured probe reflectance spectra for co-circularly polarized pump and probe when the lower mode is excited. The probe time delay is set to 0.0 ps. (a) δ=1.0 meV, I_p=0.4 (solid), 2.0 (dashed), and 6.8 (dashed-dot) μJ/cm^2 per pulse. (b) δ=0.5 meV, I_p=0.8 (solid), 2.7 (dashed), and 8.2 (dashed-dot) μJ/cm^2 per pulse. (c) δ=0.0 meV, I_p=0.8 (solid), 3.4 (dashed), and 7.2 (dashed-dot) μJ/cm^2 per pulse. (d) δ=-1.0 meV, I_p=0.4 (solid), 2.0 (dashed), and 6.4 (dashed-dot) μJ/cm^2 per pulse.

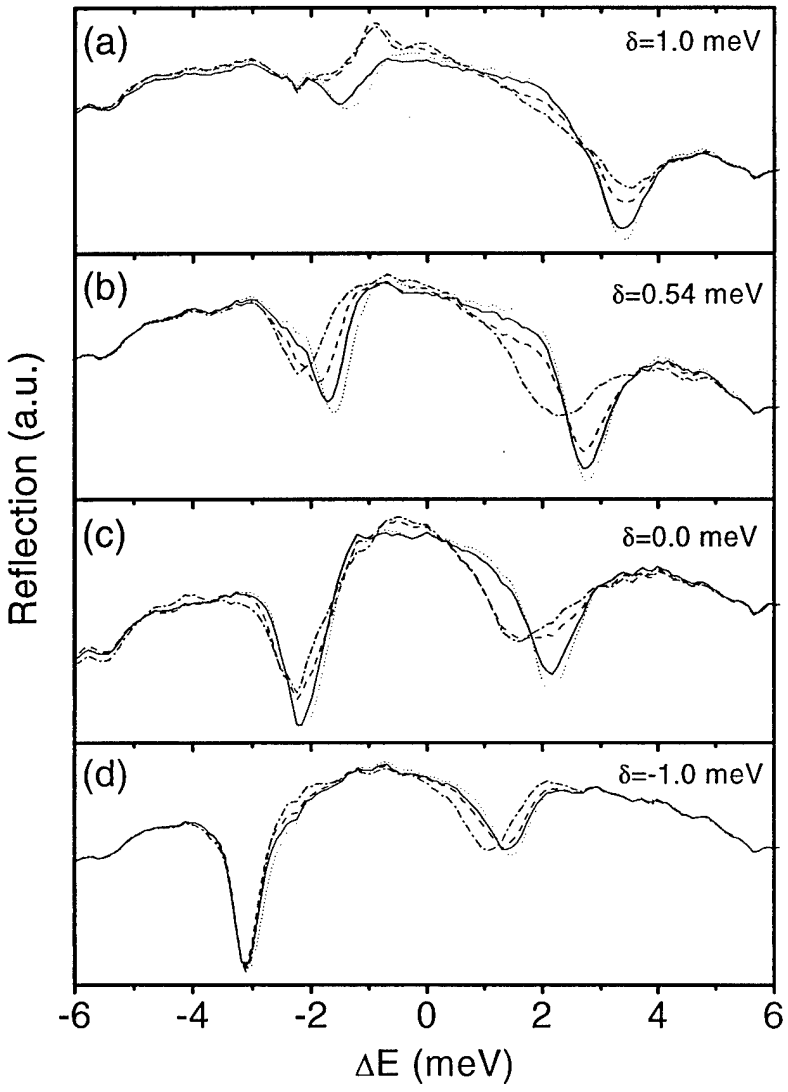

Figure 6: Measured probe reflectance spectra for cross-circularly polarized pump and probe when the lower mode is excited. The probe time delay is set to 0.0 ps. (a) δ=1.0 meV, I_p=0.8 (solid), 4.1 (dashed), and 8.2 (dashed-dot) μJ/cm^2 per pulse. (b) δ=0.5 meV, I_p=0.8 (solid), 2.0 (dashed), and 8.2 (dashed-dot) μJ/cm^2 per pulse. (c) δ=0.0 meV, I_p=0.8 (solid), 4.1 (dashed), and 8.2 (dashed-dot) μJ/cm^2 per pulse. (d) δ=-1.0 meV, I_p=0.4 (solid), 0.8 (dashed), and 6.4 (dashed-dot) μJ/cm^2 per pulse.

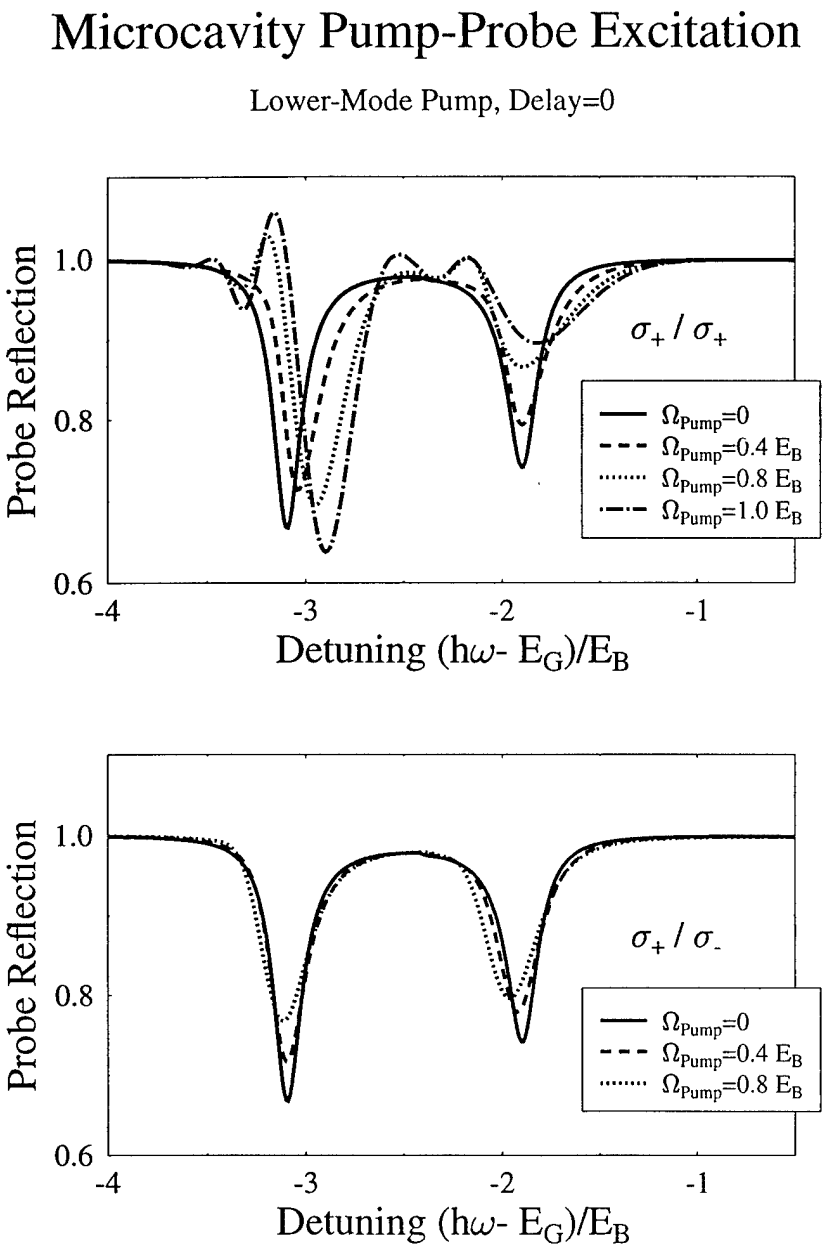

Figure 7: Calculated probe reflectivity spectra based on the second-order Born approximation

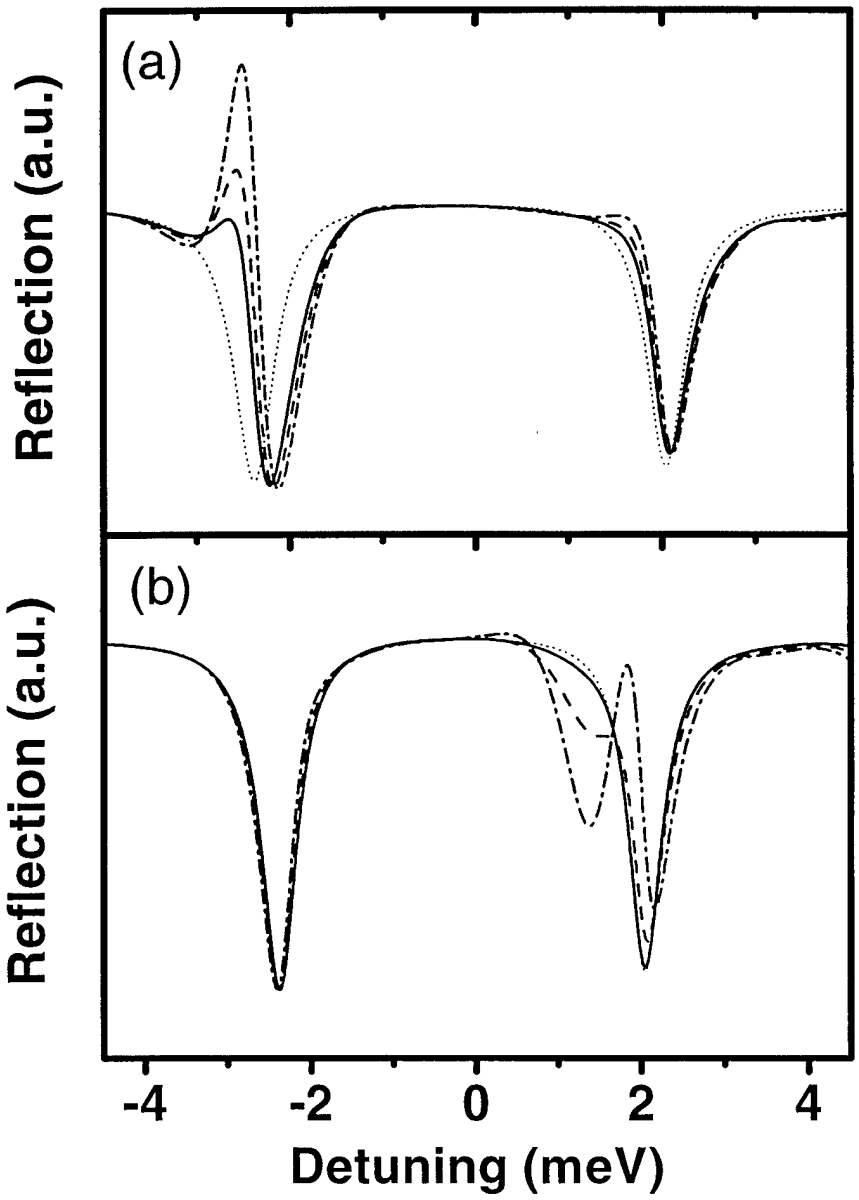

Figure 8: Calculated probe reflectivity spectra based on $\chi^{(5)}$ formalism. (a) co-circular (b) cross-circular

(propagating modes interfere). This effect is not present for cross-circular excitation due to the absence of population pulsations (and self-diffraction) for this geometry. Co-circular polarization leads to a stronger saturation of the upper mode than cross-circular polarization (in agreement with the corresponding experimental figures), because ,for cross-circular polarization, part of the dephasing-terms do not contribute as a result of their spin dependence. Ever for strong pumping and cross-circular polarization, two reflection dips are present (broadening with nearly constant splitting). Co-circular exciation leads to a pronounced blue shift of the normal-mode peaks whereas for cross-circular excitation only a weak red shift occurs (in nice agreement with the experiment and our previous QW results). The bi-exciton resonance for cross-circular configuration does not appear in 2nd Born calculations. The second Born approximation contains Coulomb interaction terms up to quadratic order in the screened Coulomb interaction, and more than three particle scattering is neglected. Thus, bi-exciton bound state does not appear in the approximation.

Figure 8 shows the calculations of the $\chi^{(5)}$ formalism. The gain peak at the red side of the lower mode is reproduced for co-circular polarization. For cross-circular configuration, the bi-excitonic mode appears at the red side of the upper mode. The theory does not represent the line shift and the strong saturation observed in the experiment, because the $\chi^{(5)}$ formalism includes only the purely coherent contributions and no scattering term contributing the saturation is included.

The second-order Born approximation as well as the $\chi^{(5)}$-treatment nicely reproduce that for co-circular polarization the gain peak near lower mode increases at elevated pump intensities. The additional broadening due to interaction-induced dephasing, which results in an initial decrease of the lower-mode peak for moderate pump intensities as well as the proper order of magnitude for lineshift and broadening are only reproduced by the calculation in Born approximation. However, this model cannot describe the emergence of a sidepeak of the upper mode for cross-circular polarization as an indication of the biexcitonic resonance. This feature is well reproduced in the $\chi^{(5)}$-calculation and is even visible in a calculation on the $\chi^{(3)}$ level.

3.5 Temporal Evolution of NMC Nonlinearities

The normal-mode spectrum itself reflects the frequency components contributing to the time resolved probe signal. The dynamics of the normal modes can be accessed by varying the delay between the pump and probe pulses. Figure 9 shows the time-resolved differential probe reflection (DR) spectra for various spectral shapes of the pump pulse. The pump spectra are shown in Fig. 9. When both modes are pumped (Fig. 9(b)), fast temporal oscillations of the DR around zero pump-probe delay can be observed. The oscillation period of 0.9 ps corresponding to the Rabi splitting of the normal modes. The oscillation amplitude is much stronger in the lower mode than in the upper mode since in connection with an asymmetric exciton spectrum the upper mode exhibits a stronger brodening [6]. For lower-mode excitation (Fig. 9(c)) the DR signal decays within a few picoseconds and the upper mode signal is much weaker than the lower mode signal. Since in this case the pump spectrum has strongly reduced overlap with the QW exciton absorption, the frequency components in the pump-induced polarization corresponding to absorptive states are much weaker and carier scattering is strongly suppressed. Only a small portion of incoherent carriers can be excited and the major part of the coherent pump-induced polarization decays radiatively within 5 ps. At longer time delay, the nonlinear response for both and upper mode pumping (Fig. 9(b) and (d)) is much stronger than for lower mode pumping because of the higher incoherent population.

Dynamics of the fast oscillation and the gain peak at the lower mode for both-mode pumping is shown in Fig. 10. The reflection spectra of the polariton modes are demonstrated between t=-4.67 and 1.33 ps with a time step of 0.33 ps. The fast oscillation in Fig. 5(b) is clearly seen in the lower mode reflection spectra, though it is not quite clear in the upper mode. Besides, as time goes by, the

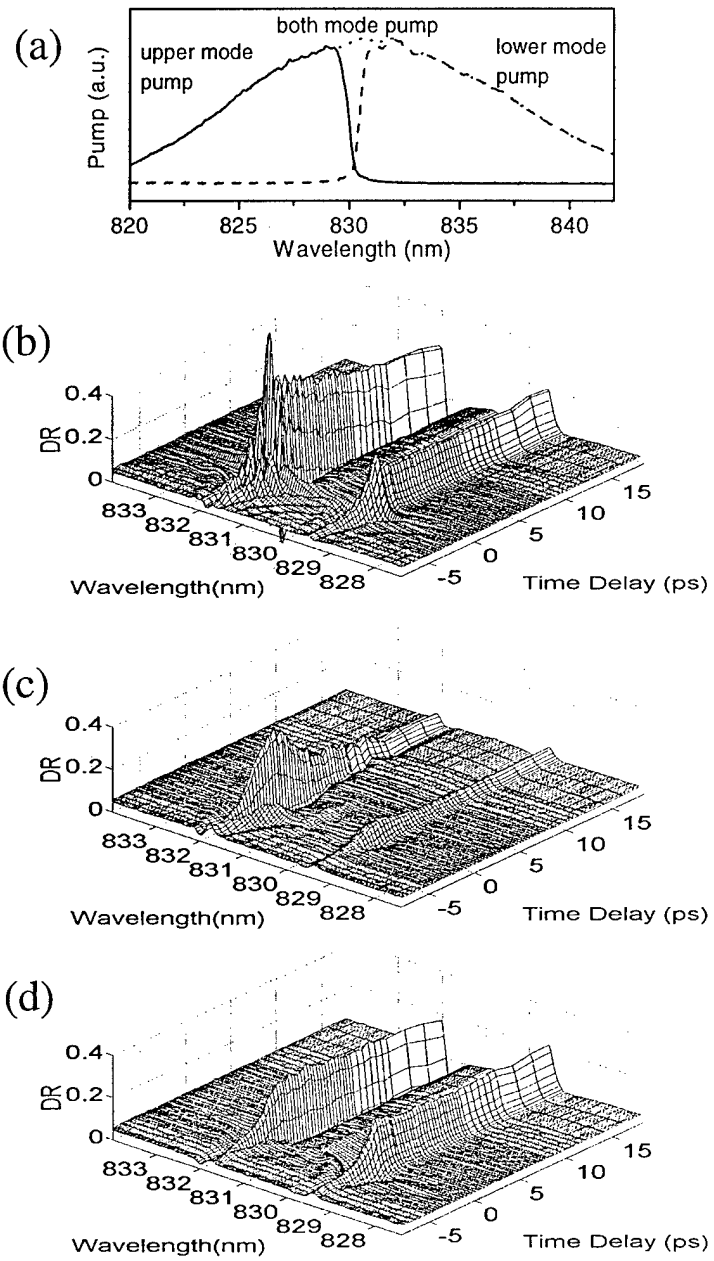

Figure 9: (a) Pump spectra for both-mode, upper mode and lower mode pumping. Time-resolved differential reflectivity spectra of polariton modes in the QW microcavity when (b) both modes, (c) the lower mode, and (d) the upper mode is pumped. Pump fluence is 4.8 μJ/cm^2 per pulse before the spectral filtering. The pump and probe pulses are co-circularly polarized.

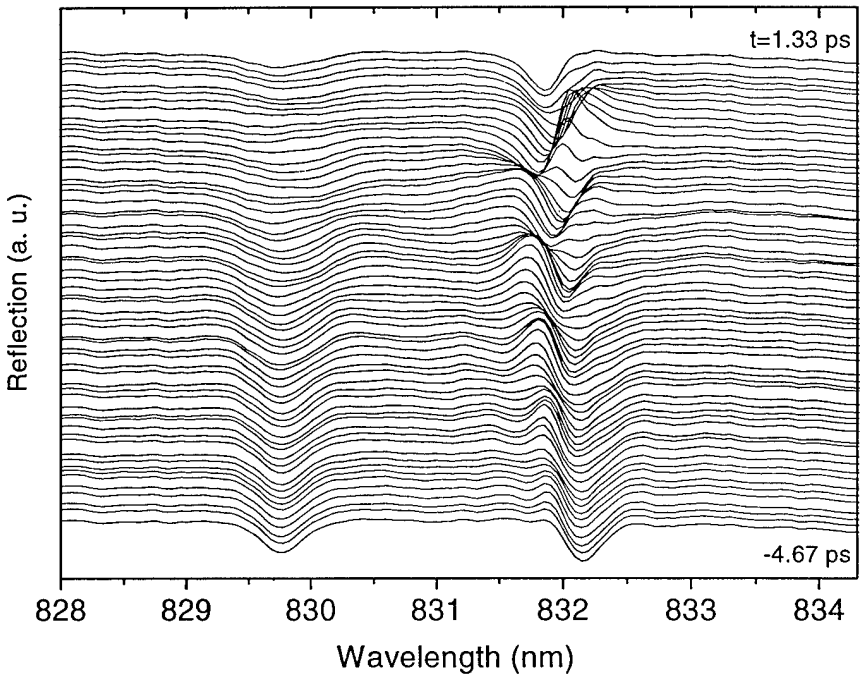

Figure 10: Reflection spectra of the polariton modes for various time delays between the pump and probe pulses from -4.67 to 1.33 ps. Each spectrum is vertically displaced, and the time delay between the sectra is 0.33 ps.

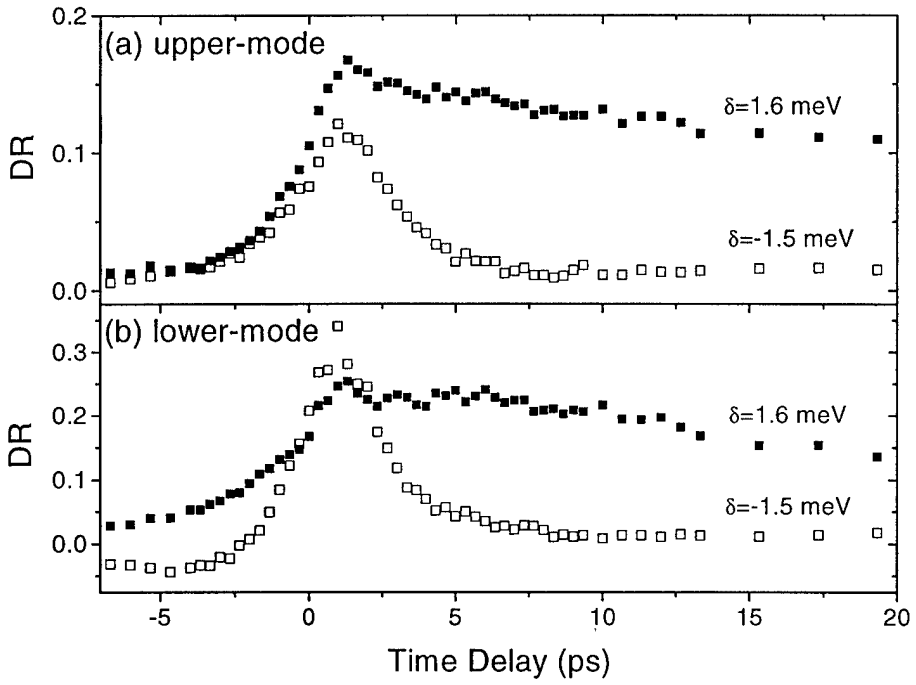

Figure 11: Time-resolved differential reflectiviy at (a) the upper and (b) the lower mode resonance wavelength. The cavity detuning (δ) is -1.5 meV(open square) and 1.6 meV(solid square). The resonance wavelength of the lower mode is 832.72nm (δ=-1.5 meV) and 831.52 nm (δ=1.6 meV), and the resonance wavelength of the upper mode is 829.93 nm (δ=-1.5 meV) and 828.81 nm (δ=1.6 meV).

polariton modes are shifted to the blue side, because the exchange interaction terms contributing to the nonlinear signal always produces a blue shift of the exciton. Around t=0, temporal evolution of the gain peak at the red side of the lower mode is shown. The peak grows and decays within a few picoseconds, and the peak shifts to the red side as time goes by.

We observed the time-resolved DR for the lower mode pumping at the normal mode resonance wavelengths when the cavity detuning is -1.5 and 1.6 meV in order to study the decay of the DR signal (Fig. 11. In the negative (positive) detuning, the proportion of the cavity photon (exciton) mode in the lower mode polariton is larger than of the exciton (cavity photon) mode. Thus, the radiative decay time of the lower mode polariton in the negative detuning is faster than in the positive detuning.

3.6 Conclusions

The strong broadening and lineshift effects, which are clearly observable in the experimental spectra for elevated pump intensities are well reproduced with the theory in second-order Born approximation while the $\chi^{(3)}$ and $\chi^{(5)}$-treatment leads only weak shift and broadening contributions. Both theories can account for the gain at the red side of the lower normal mode for co-circular optical polarization as a coherent scattering of the pump signal into probe direction. Only the full treatment of Coulomb correlations up to $\chi^{(3)}$ and $\chi^{(5)}$ contributions reproduces the biexcitonic sidepeak in the normal-mode spectra for cross-circular polarization and zero pump-probe delay, which is practically absent for a pump-probe delay of 1 ps.

References

[1] Y. -S. Lee *et al.*, Optics & Photonics News **9**, 60 (1998).

[2] Y. -S. Lee *et al.*, Phys. Stat. Sol. (B) **221**, 121 (2000).

[3] Y. -S. Lee *et al.*, Appl. Phys. Lett. **78**, 3941 (2001).

[4] S.L. Palfrey and T.F. Heinz, J. Opt. Soc. Am. B **2**, 674 (1985).

[5] C. Weisbuch *et al.*, Phys. Rev. Lett. **69**, 3314 (1992).

[6] G. Khitrova *et al.*, Rev. Mod. Phys. **71**, 1591 (1999).

[7] C. Ciuti *et al.*, Phys. Rev. B **58**, R10123 (1998).

[8] T. Baars *et al.*, Phys. Rev. B **61**, R2409 (2000).

[9] P. Borri *et al.*, Phys. Rev. B **61**, R13377(2000).

[10] C. Ell *et al.*, Phys. Rev. Lett. **85**, 5392 (2000).

[11] J. Bloch and J. Y. Marzin, Phys. Rev. B **56**, 2103 (1997).

[12] B. Sermage *et al.*, Phys. Rev. B **53**, 16516 (1996).

[13] M. Kuwata-Gonokami *et al.*, Phys. Rev. Lett. **79**, 1341 (1997).

[14] J. Baumberg *et al.*, Phys. Rev. Lett. **81**, 661 (1998).

[15] C. Sieh, T. Meier, F. Jahnke, A. Knorr, S.W. Koch, P. Brick, M. Hübner, C. Ell, J.P. Prineas, G. Khitrova, and H.M. Gibbs, Phys. Rev. Lett. **82**, 3112 (1999).

[16] C. Sieh, T. Meier, A. Knorr, F. Jahnke, P. Thomas, and S.W. Koch, European Physical Journal B **11**, 407 (1999).

[17] R. Binder, S.W. Koch, M. Lindberg, W. Schäfer, and F. Jahnke, Phys. Rev. B **43**, 6520 (1991).

[18] P. Meystre and M. Sargent III, Elements of Quantum Optics, Springer, New York (1991).

[19] F. Jahnke, M. Kira, and S.W. Koch, Z. Physik B **104**, 559 (1997).